Design Principles for High H_2 Storage Using Chelation of Abundant Transition Metals in Covalent Organic Frameworks for 0-700 bar at 298K

Yohanes Pramudya[†,‡] and Jose L. Mendoza-Cortes[*,†,‡]

Department of Chemical & Biomedical Engineering, FAMU-FSU College of Engineering, Florida State University, Tallahassee FL, 32310, USA, and Scientific Computing Department, Materials Science and Engineering Program, High Performance Material Institute, Condensed Matter Theory-National High Magnetic Field Laboratory, Florida State University, Tallahassee FL, 32310, USA

E-mail: jmendozacortes@fsu.edu

Abstract

Physisorption is an effective route to meet hydrogen gas (H_2) storage and delivery requirements for transportation because it is fast and fully reversible at mild conditions. However, most current candidates have too small binding enthalpies to H_2 which leads to volumetric capacity less than 10 g/L compared to the system target of 40 g/L at 298K. Accurate quantum mechanical(QM) methods were used to determine the H_2

[*]To whom correspondence should be addressed

[†]Department of Chemical & Biomedical Engineering, FAMU-FSU College of Engineering, Florida State University, Tallahassee FL, 32310, USA

[‡]Scientific Computing Department, Materials Science and Engineering Program, High Performance Material Institute, Condensed Matter Theory-National High Magnetic Field Laboratory, Florida State University, Tallahassee FL, 32310, USA

binding enthalpy of 5 linkers which were chelated with 11 different transition metals (Tm), including abundant first row Tm (Sc through Cu); totaling 60 molecular compounds with more than 4 configurations related to the different number of H_2 interact with the molecular compound. It was found that first row Tm gave similar and sometimes superior van der Waals interactions with H_2 than precious Tm. Based on these linkers, 30 new covalent organic frameworks (COFs) were constructed. The H_2 uptakes of these new COFs were determined using Quantum Mechanics (QM) based force fields and Grand Canonical Monte Carlo (GCMC) simulations. For the first time, the range for the adsorption pressure was explored for 0-700 bar and 298K. It was determined that Co, Ni, and Fe based COFs can give high H_2 uptake and delivery when compared to bulk H_2 on this unexplored range of pressure.

INTRODUCTION

One of the main obstacle to use H_2 as an alternative energy source is the difficulty of storage at operational temperature (233K to 358K). The U.S. Department of Energy (DOE) has set the 2020 uptake targets of 5.5 weight percent (wt %) and 40 g/L at 233-358 K (ultimate target 7.5 wt % and 70 g/L).[1] To achieve this goal, between chemisorption and physisorption, it is believed by the authors that physisorption is the best route because it is fully-reversible and has fast kinetics at the desired conditions. Severals researchers have found that it is necessary to keep a relatively constant heat of adsorption (Q_{st}) as the H_2 uptake increases in order to have an efficient charge/discharge cycle, which is a requirement of the DOE target.[2,3] Current materials have been able to reach values for heat of adsorption Q_{st} less than 8 kJ/mol at ambient conditions, and this magnitude decays as the first sorption sites get saturated due to the entropic change at higher temperatures.[3,4] Thus, sorption sites that have stronger affinity and that are able to accommodate multiple H_2 molecules are needed. Several theoretical studies of proposed materials showed stronger interaction between H_2 and the host materials, although they have not been experimentally

synthesized.[4–7] We proposed that using chelation of Tm inside porous materials can reach a practical volumetric and gravimetric H_2 storage.[8–10] Our previous attempts have focused on using precious late transition metals (Tm) such as Pd and Pt.[10] However, in this work, the chelation with abundant first row Tm (Sc to Cu) is explored.

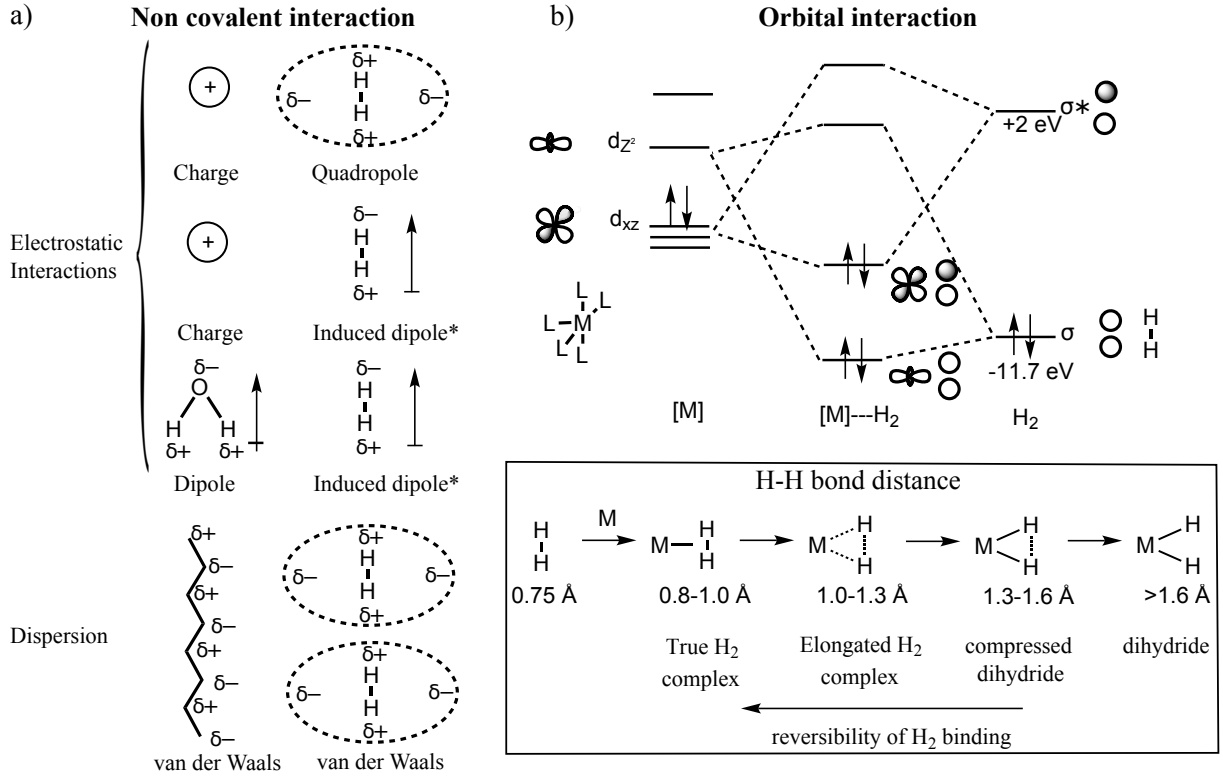

(*A strong external field is needed to create a dipole in H_2)

Figure 1: Fundamental interactions of H_2 with other materials:[11,12] a) non covalent interaction caused by electrostatic interactions including van der Waals interaction and b) The molecular orbital diagram between Tm and H_2, the inset showing the H-H bond distances (from crystallography and NMR) are adapted from Kubas et al.[11,13]

Table 1: Types of interactions for H_2 which can be used for tuning the $\Delta H^\circ_{\mathrm{bind}}$.

Interaction (material–H_2)	**Energy dependence**	**Typical values (kJ/mol)**
charge-quadropole	$\propto 1/r^3$	~ 3.5[11]
charge-induced dipole[a]	$\propto 1/r^4$	~ 6.8[11,12]
dipole-induced dipole[a]	$\propto 1/r^5$	~ 0.6[3]
van der Waals	$\propto 1/r^6$	$\sim 5-6$[13–16]
orbital interaction	$<$ vdW radii	$\sim 20-160$[11,13]

[a] Dipole moment in H_2 can be induced by strong electric field.

Fundamental H_2 interactions

At the fundamental level, H_2 can interact with other atoms, molecules, and solids via non covalent (van der Waals and electrostatics) and orbital interactions; which are summarized in Figure 1 and Table 1.[11–13] The total interactions of the H_2 molecule with a molecule or solid determines the binding energy (ΔH°_{bind}).

Non covalent interactions. Most interactions in bulk H_2 are related to their quadrupole moment due to the non-spherical nature of H_2; so-called quadropole-quadropole interactions. Hydrogen gas can also interact with ions and create charge-quadrupole interaction. H_2 can have an induced-dipole moment and generate other interactions such as charge-induced dipole and dipole-induced dipole with a strong external field.[11,12] The other ubiquitous non covalent interaction is due to van der Waals force which is responsible for the interaction of H_2 with most molecules and materials, e.g. carbonaceous compounds such as graphite and carbon nanotubes.[3] The typical values of each of these interactions are less than 7 kJ/mol (Table 1).

Orbital interactions. Orbital interactions require either a very high-pressure of 490 GPa[17] on H_2 alone or d-orbitals of Tm to appear.[13–16] The use of the d-orbital of Tm is the most obvious choice because of the constraint for practical purposes of using up to 700 bar of pressure. The orbital interactions have a different magnitude depending on the Tm and the ligands used, and ultimately affect the H-H bond. The greater the interaction, the more the H-H bond elongates and less reversible the binding becomes. The typical values for these types of interactions is 20-160 kJ/mol (Table 1).

In principle, transition metals chelated to organic linkers present in COFs can have different kinds of interactions and binding sites with H_2. The combination of different strong interactions with H_2 are needed to achieve high uptake. These interactions can be tuned to modify the binding energy (ΔH°_{bind}) of H_2 to a material in order to achieve the uptake goals of the Department of Energy (DOE). A first estimation of the numerical value of this ΔH°_{bind} can be done by a Langmuir Toy Model. The insights obtained can then be used to create

the best porous materials.

DOE Targets and The Connection to The Binding Energies of H_2 (ΔH°_{bind})

Langmuir Toy Model was used to estimate the uptake and delivery of hydrogen molecules at 0-700 bar pressure range. The purpose of using this model was to gain an intuition on this phenomenon and to estimate possible ideal values for ΔH°_{bind}. Using this model, it is shown that the value of the ΔH°_{ads} affects the delivery amount of H_2 at 298 K (Figure 2). This model also shows that the optimal strength value is between 7-15 kJ/mol. Based on this result, the next obvious step is finding Tm chelated with ligands that can have a binding enthalpy between 7 to 15 kJ/ mol in order to get the optimal delivery amount for the DOE targets by exploiting most of the different types of interactions that H_2 can have within the porous framework.

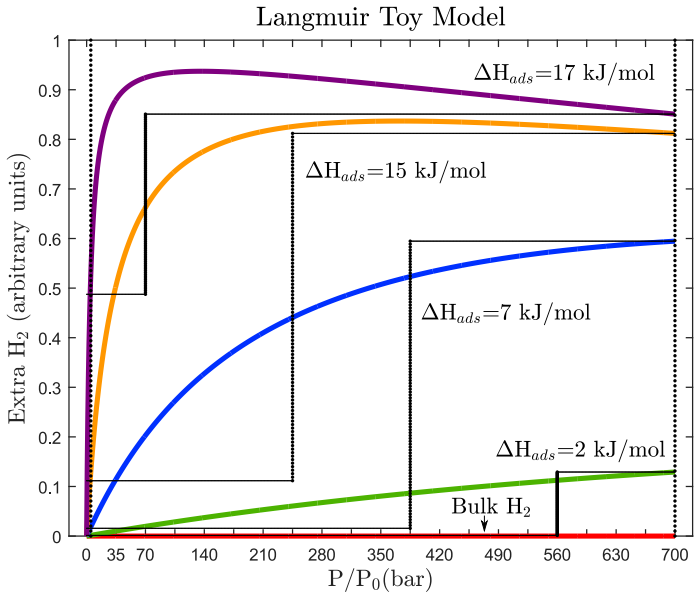

Figure 2: The normalized extra uptake for four different adsorption enthalpies at 298K is shown using the Langmuir Toy Model. The magnitude of the interaction has a strong effect on the amount that can be delivered between 3 and 700 bar. In this model, a simple approximation is used; $\Delta H^{\circ}_{bind} \approx \Delta H^{\circ}_{ads}$. P/P_0 is the pressure relative to normal atmospheric pressure with $P_0 = 1$ bar.

As shown in Figure 1 and Table 1, non-covalent interactions (electrostatic and van der Waals) have a typical binding enthalpy (ΔH°_{bind}) of less than 7 kJ/mol. This has been proven to be insufficient for achieving the optimal adsorbent-H_2 interaction.

Although ΔH°_{bind} represent the interaction only at one specific adsorption site in one ligand, in this work, it is proven that calculating ΔH°_{bind} is usually a good approximation to the experimental value of isosteric heat of adsorption Q_{st} obtained for COFs if the adsorbent material is replete with many similar adsorption sites. Thus the connection from a molecular calculation (i.e. ligand) to the periodic material (COF) using this molecule as a building block can be used to find promising linkers for the design of porous COFs.

This paper is formatted as follows; in the Materials and Methods section, the details of the quantum mechanical (QM) methods, the force field development and the grand canonical schemes are presented. In the Results and Discussion section, the molecular QM results are presented, followed by the periodic QM calculations and the GCMC results for 30 newly designed COFs in the 0-700 bar pressure range. The validity of the estimation for Q_{st} from the ΔH°_{bind} is also discussed. Finally, in the summary, the design principles for new porous materials for H_2 storage are presented.

MATERIALS AND METHODS

Quantum Mechanical Calculations

Molecular Quantum Calculations. Molecular Quantum Calculations at the hybrid-DFT level were performed to calculate the interactions of the different linkers with H_2. These calculations were performed using the B3LYP functional with the D3 corrections as implemented in the Amsterdam Density Functional (ADF)[18] code. This implementation is based on Slater-Type Orbital (STO) basis sets instead of Gaussian-Type Orbital (GTO) basis sets.[19] The STO basis sets give relatively consistent and rapidly converging results. The valence Triple Zeta + 1 Polarization functions (TZP) were used for geometry optimization

and calculation of the binding enthalpy. The unrestricted open shell procedure for self-consistent field calculation was used for all spin states.

The following expression was used to obtain the ΔH°_{bind} for each H_2 binding site:

$$\Delta H^{\circ}_{bind} = \Delta H^{\circ}_{Linker+H_2} - \Delta H^{\circ}_{Linker} - \Delta H^{\circ}_{H_2}, \quad (1)$$

where $\Delta H^{\circ}_{Linker+H_2}$ is the enthalpy for the complex formed between linker-H_2, $\Delta H^{\circ}_{Linker}$ is the enthalpy of the molecular linker alone, and $\Delta H^{\circ}_{H_2}$ is the enthalpy of the H_2 molecule alone. To calculate the enthalpy, electronic (elec), vibrational (vib), and zero point vibration energy (ZPE) are considered; thus for each compound $\Delta H^{\circ} = E_{elec} + ZPE + H^{\circ}_{vib}$.

Periodic Quantum Mechanics Calculations. Periodic quantum calculations at the Density Functional Theory (DFT) level were carried out with the PBE functional and D3 dispersion correction with Becke-Jonson (BJ) damping. The Vienna Ab initio simulation package (VASP) code was used. Full geometry optimizations were performed (ISIF=3) where both atoms and volume of the crystals are optimized. Other parameters included: fully automatic optimization projection done in real space (LREAL=Auto), allowed error in total energy for electronic self consistent (SC)-loop (EDIFF=10^{-4}), maximum allowed force between ionic relaxation (EDIFFG=-2×10^{-3}), Gaussian smearing (ISMEAR=0), spin polarized calculation (ISPIN=2), cut-off energy for plane wave basis set (ENCUT= 520 eV), kinetic energy cut-off for augmentation charges (ENAUG = 1020 eV), number of k points (KPOINTS=$2 \times 2 \times 2$) and D3 dispersion correction with BJ damping (IVDW =12). Periodic QM calculations were used to optimize the structure of COF-300, COF-301, COF-320, COF-322, COF-330, COF-333, COF-340, COF-350, and their chelated transition metal structures. The primitive cell of each Covalent Organic Framework already has a very big number of atoms from 178 atom in COF-301 to 278 atoms in COF-340. Thus, it does not need a high number of k points.

QM based Force Field

To describe the best H_2 adsorption, the force fields with the parameters for interactions between organics (H, C, N, O) and molecular hydrogen are developed. The Morse potential was selected over alternatives for its comparative accuracy and stability over a large range of distances (r), including small r. The Morse potential has the form:

$$\boldsymbol{U}_{\mathrm{ij}}^{\mathrm{Morse}}(r_{ij}) = D\left[\left(1 - e^{-\alpha(r_{ij}-r_0)}\right)^2 - 1.0\right] \tag{2}$$

where D is the well depth, r_0 is the equilibrium bond distance, and α determines the stiffness (force constant). First, molecular quantum mechanical calculations as described in the previous section were used to compute the equilibrium energies and configurations of various molecules with molecular hydrogens. The values for fitted Ab initio based force field parameters are shown in Table 2.

Table 2: Table of parameters for the force field based on the Morse potential given in Equation (2). D is the well depth, r_0 is the equilibrium bond distance, and α determines the force constant.

Element	D_0 (kcal/mol)	α (Å^{-1})	r_0 (Å)
H_{H_2} — Co ($CoCl_2$)	0.879	0.850	2.985
H_{H_2} — Cu ($CuCl_2$)	0.818	1.462	2.931
H_{H_2} — Fe ($FeCl_2$)	1.092	1.180	3.015
H_{H_2} — Mn ($MnCl_2$)	0.994	0.990	3.015
H_{H_2} — Ni ($NiCl_2$)	1.154	1.210	3.207

Grand Canonical Monte Carlo (GCMC)

The force field based on first principles described above was used in Grand Canonical Monte Carlo (GCMC) ensemble simulations. Here, for each temperature and pressure, 5,000,000 configurations were constructed to compute the average loading for which convergence was

obtained. Every GCMC step allows 4 possible events: translation, rotation, creation and annihilation, each at equal probability.

RESULTS AND DISCUSSION

Binding Enthalpy of H_2 and linkers bounded to Tm used in porous frameworks

Generating sites for chelation leads us to develop new covalent organic frameworks (COFs) with the imine and hydrazide linkage.[20,21] Figure 3 summarizes the linkers where sites to host metals were purposely created. These linkers will be used for building COFs.[8,9] The use of bypiridine and phenanthroline as linkers in hypothetical COFs was also explored (Figure 3).

These linkers used for chelation of Tm and their binding energies to H_2 were calculated. The results are summarized in Figure 4. It was found that it is not necessary to use precious and heavy transition metals to obtain good binding energies with H_2. First row Tm (Sc to Cu) can achieve similar and sometimes superior strength of interactions than precious late transition metals (Pd and Pt). This is based on the study of binding enthalpy ΔH°_{bind} of 1 to 4 H_2 molecules interacting with 60 compounds (5 linkers combines with 11 different transition metals).

The ligands studied were: (E)-N'-benzylidene-benzohydrazide (**BBH**), (E)-2- ((phenylimino) methyl) phenol (**PIP**), (E)-N-(pyridin-2-ylmethylene) aniline (**PIA**), 2,2'-bipyridine (**BPY**), and phenanthroline (**PHEN**) (shown in Figure 3). It was found that each of these ligands alone cannot interact strongly enough with the hydrogen molecule (typical ΔH°_{bind} values are from -4 to -7 kJ/mol for the first four H_2). However, it was found that if a Tm is bound to the ligand, the H_2 interaction enthalpy increases, with some complexes having the optimal ΔH°_{bind} based on the Langmuir Toy Model to obtain the maximum delivery amount of hydrogen gas for the pressure range needed by the DOE targets at room temperature.

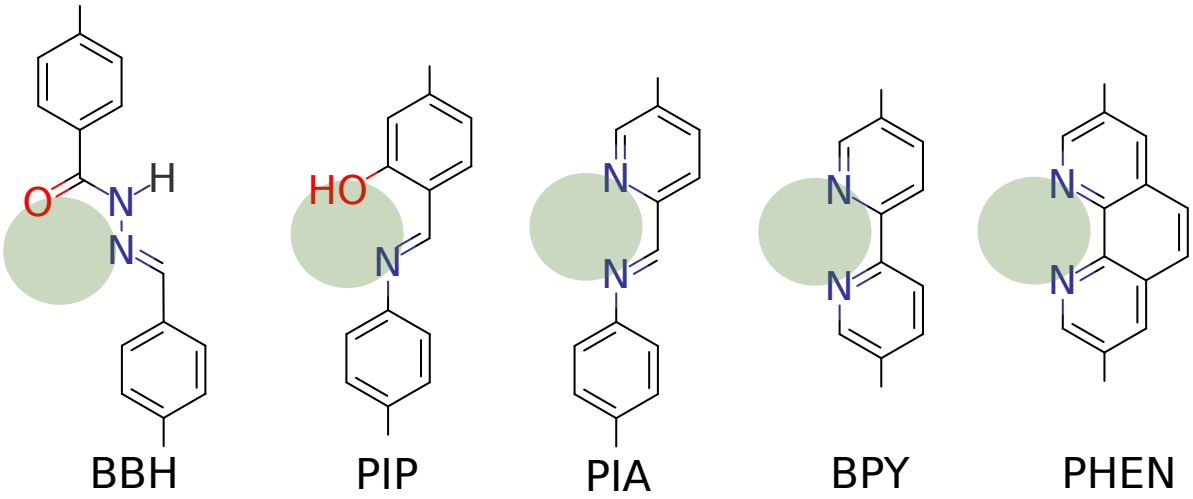

Figure 3: Linkers are used for current designed COFs where the chelation sites are shown in green circles.

It was found that the most favorable geometries given the electronic spin states were: tetrahedral (Tet) versus square planar (Sqr) when applicable or trigonal bipyramidal (Tbi) versus square pyramidal (Spy). The other geometries studied depending on the number of ligands are octahedral (Oct) and pentagonal bipyramidal (Pbi). It was also found that in general square planar coordination geometry is not required to obtain strong interactions because the tetrahedral geometry gives similar affinity for H_2. As we expected; the square geometry gives better interaction for more H_2 bonded to the complex. The pentagonal bipyramidal and octahedral geometry [**BBH**-V(V)Cl_5 and **BBH**-Ti(IV)Cl_4] would hindrance the interactions of the Tm with the H_2, however the total strength is still comparable to those interaction obtained from tetrahedral and square geometry (Figure 4). This is because of extra interactions from 2 or 3 Cl^- ions with H_2 in $TiCl_4$ and VCl_5.

For the Tm bound to these linkers, the tetrahedral geometry in general gives slightly stronger binding interaction to H_2 than the square geometry. These geometries give slightly stronger interaction than the trigonal bipyramidal, and are followed by the octahedral and pentagonal bipyramidal geometry. Thus if the gravimetric uptake needs to be optimized, lighter first row Tm with the least counter anions can be used. This will serve as a principle in the future design as a way to tune the H_2 interactions with chelated organic frameworks.

Some of the ligands have been synthesized with Tm chelation.[22–25] The initial experimental geometry was used to optimized the structure. Some of the ligands have been synthesized previously, and in some cases the chelation has been reported with Ni(II)[22], Cu(II)[23], Pt(II)[24], and Pd(II)[25]. The initial experimental geometry was used when available to chelate other Tm. Pd(II) and Pt(II) were included to compare precious late transition metal to early Tm interaction (Figure 4). Further details about the electrons quantum properties of the interactions will be published elsewhere.

Ligand containing the hydrazide (BBH) binding group. The first linker calculated was the hydrazide containing linker; (E)-N'-benzyli-denebenzo-hydrazide (**BBH**) shown in Figure 3. COF-42 and COF-43 were made by this connectivity.[20] With the purpose of knowing which transition metal would have the best binding enthalpy to H_2, the interactions of such compounds using first row transition metals (Sc to Cu) as well as Pd and Pt were calculated. The results are shown in Figure 4.

For all these cases, the H_2 does not bind chemically to the Tm. No strong interaction between the first H_2 with any of these first row transition metals were found, only η^2-H_2 interaction ($\Delta H^\circ_{\text{bind}} \sim 15 - 20$kJ/mol). The rest of the Tm studied exhibit a very similar behavior with $\Delta H^\circ_{\text{bind}}$ that ranges from 8-12 kJ/mol for the 1^{st}-4^{th} interacting H_2. The H-H bond is not affected by more than 0.1 Å.

While this study focused on the ground state geometry for the Tm interacting with H_2, the effect of having other spin states for the same oxidation state was also explored. The trend is consistent with the high spin Tm interacting more strongly with H_2 than the low spin analog (SI), however the high spin is not always the ground state.

Ligand containing the Imine-Pyridine (PIA) binding group. Other efforts to generate chelation sites made use of the linker (E)-N-(pyridin-2-ylmethylene) aniline (**PIA**) to construct a MOF.[8] The chelation of this linker with different Tm was also studied in this work and the results are shown in Figure 4. It was found that almost all the compounds of

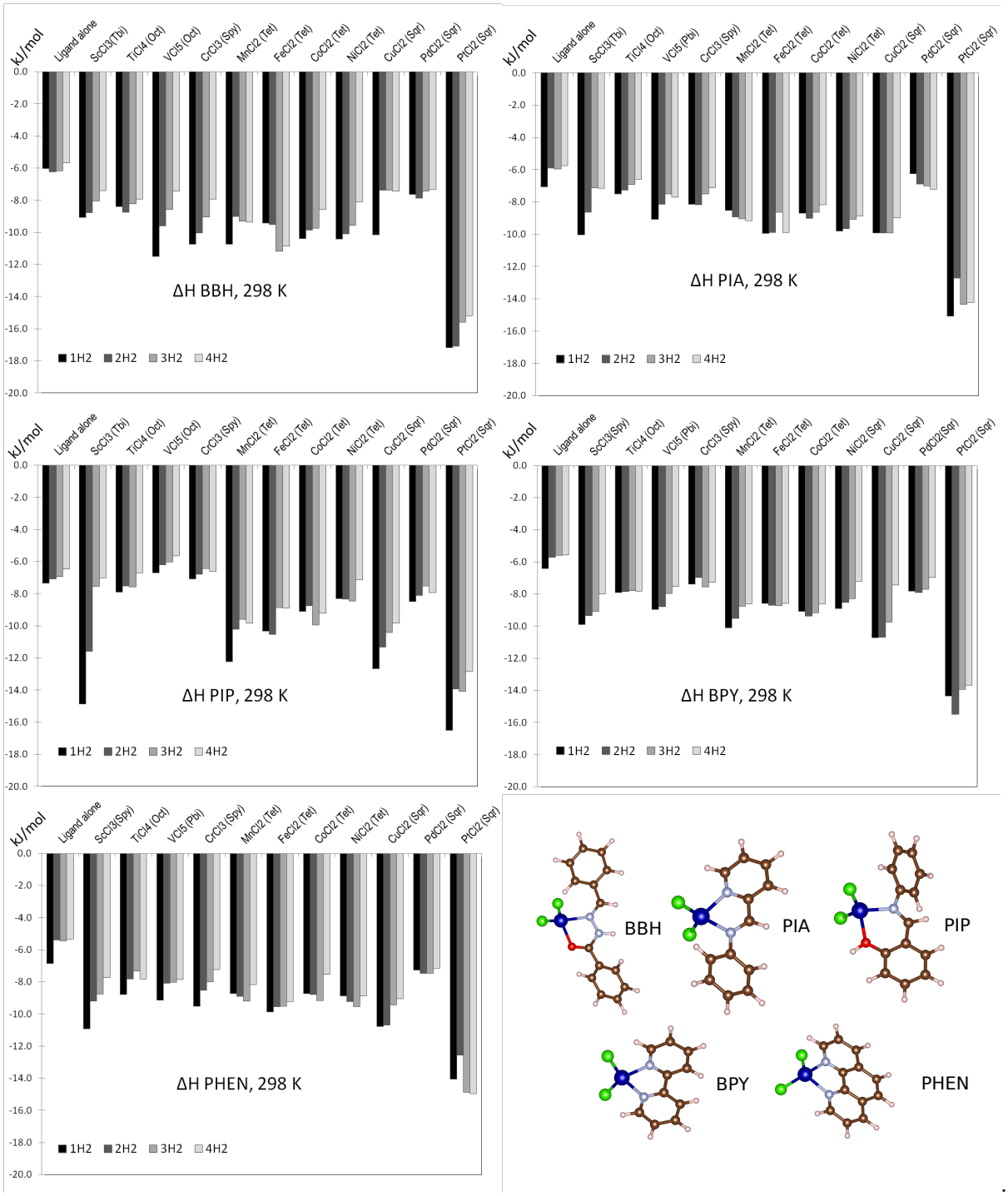

Figure 4: Binding enthalpies ΔH°_{bind} calculated using molecular QM at 298K obtained for **BBH**, **PIA**, **PIP**, **BPY**, and **PHEN** , pure ligand and their chelated analogs interacting with up to four H_2.

the form **PIA** + $Tm(n)Cl_n$ do not bind chemically to the first H_2 and have a ΔH°_{bind} that ranges from -8 to -12 kJ/mol for the 1st-4th interacting H_2. Also, in general the H-H bond is

not perturbed significantly. Thus the H_2 have mild interactions with Tm in the ideal range for maximum uptake under the assumption of the Langmuir Toy Model presented in this work. The results suggest that any of the Tm presented here with their respective oxidation states should give an optimal uptake amount of H_2, given that the porous structure is formed mostly out of these Tm sites.

Ligand containing the Imine (PIP) binding group. Previous efforts to make other kinds of COFs developed the imine connectivity in COF-301.[21] The main linker used for the synthesis is (E)-2-((phenylimino)-methyl) phenol (**PIP**) (Figure 3). The chelation of Tm; Sc to Cu as well as Pd(II) and Pt(II) with this linkers was further explored. The results are shown in Figure 4. It was found that only Pt(II) and Sc(III) interact strongly (< -15 kJ/mol) with the 1st H_2 η^2-Tm. The other Tm have interactions in the ideal ΔH°_{bind} range of 8-12 kJ/mol calculated with the Langmuir Toy Model.

Ligand containing the bipyridine (BPY) group. At the beginning, the hypothesis was that the square geometry Tm was essential to obtain the maximum number of interacting Tm with acceptable strength versus tetrahedral or other geometries. Thus, the Cambridge structural database (CSD) was consulted in the search for the square planar geometry present in Tm with pyridine ligands. **Bipyridines** were proposed as candidates ligands because these ligands are chelated constantly and thus are good possibilities to have a chelated framework (Figure 3). The linker studied with this approach was 2,2'-bipyridine (**BPY**). For this linker, Tm have a relatively constant values over the first four H_2, which is desirable for a host in real applications, the interaction is in the range of 8-12 kJ/mol showing the utility of chelation as a way to improve the interaction with Tm. Based on this results, none of the first row Tm form η^2-Tm interaction in this ligand.

Ligand containing phenanthroline (PHEN) group. The last linker considered was phenanthroline (**PHEN**) which has coordination properties similar to **BPY**. The binding

enthalpy to the H_2 when using **PHEN** is very similar to other ligands. The relatively flat binding enthalpy gives a non monotonic trend relative to the number of H_2 within the typical values of absolute error bar in ADF.[19] The Triple Zeta Function (TZP) in ADF for Pt (II) is still under development and show an anomaly in the 3^{th} and 4^{th} H_2 binding enthalpy.

Design of expanded imine based COF-300 containing metal binding sites. The previous ligands (**BBH**, **PIP**, **PIA**, **BPY**, **PHEN**) were used as linkers in the creation of new COFs. The ligands were made into periodic structure through the formation of imine bonds (Figure 5 and Figure 6). In the design of the COFs through imine formation, the **dia-c5** topology (diamond-topology with 5-fold interpenetration) was considered, since similar structure is observed in COF-300.[21] To build each structure, the corresponding space group and the irreducible representation of the ligand were used (Figure 5 and Table 3). Once the COFs are created, the structure is minimized using periodic QM (VASP with PBE-D3). Table 3 summarize the linkers used, estimated pore size, and metal binding site for a series of COFs.

Table 3: Summary of linker used, calculated pore size, and metal binding site for a series of COFs.

COF-n	Link	Pore size	Metal binding site
COF-300	1+2	10	N/A
COF-301	1+3	6	imino-hidroxi
COF-320	1+4	14	N/A
COF-322	1+5	15	bipyridine
COF-330	1+7	16	phenanthroline
COF-333	1+6	14	iminopyridine
COF-340	1+8	22	phenanthroline
COF-350	1+9	9	hydrazide

H_2 uptake of chelated Tm in imine-COFs. The developed FF parameters along with GCMC were used to calculate the isotherm for all the imine-COFs containing Tm. Other COFs were constructed using the same principle and are shown in Figure 7. The imine-COFs

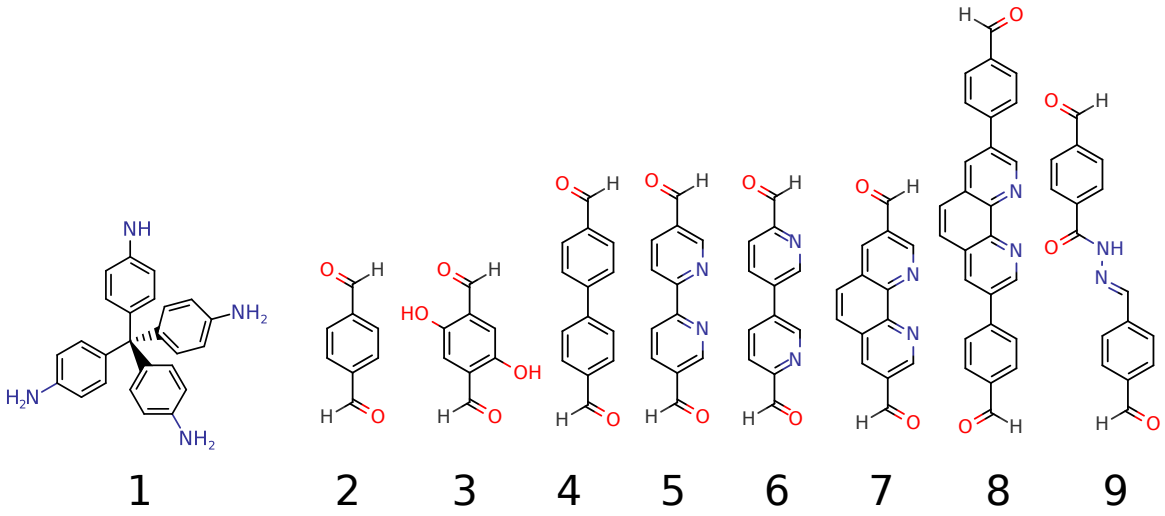

Figure 5: Building block being used for the construction of new COFs through imine bond formation.

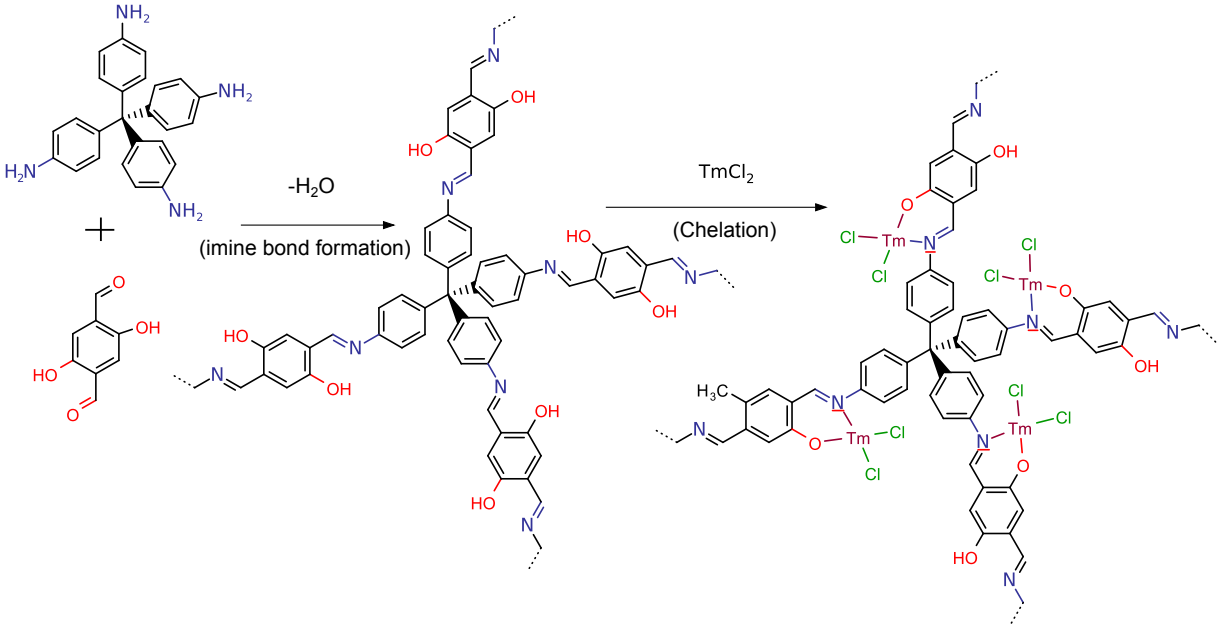

Figure 6: Approach for the creation of a COF and a *posteriori* chelation with transition metals (Tm).

were designed by intending the dehydration reaction shown in Figure 6. The strategy for metalation of the pure COFs is post-metalation of the framework and it exemplified by COF-301 after adding $TmCl_2$. As expected the uptakes increase dramatically by 2-4 folds with the presence of $TmCl_2$ to form COF-322-$TmCl_2$, COF-330-$TmCl_2$ and COF-333-$TmCl_2$ but they still do not perform as well as COF-301-$TmCl_2$ (Figure 8 and Table 4). Other COFs

have less performance than COF-301 due to the bigger pore size, which wastes space and has a less cooperative effect. They all have the same trend at low pressure (0-100 bar), porous materials always give higher uptake than bulk H_2. At higher pressure (100-700 bar), porous materials may not benefit the total uptake compared to bulk H_2, and it depends on the pore size and the strength of the transition metal interaction with the H_2. Bigger pore size may still accommodate more H_2 at higher pressure and Co(II), Ni(II), Fe(II), and Cu(II) still can compensate for small pore size that limits the surface area of porous material at higher pressure (Figure 7 and Figure 8). Chelated Co in COF-301 has maximum higher uptake relative to bulk H_2 22.2 g/L at 120 bar and decreases as the pressure increases but still has more than 12 g/L advantage over bulk H_2 at 700 bar. Chelated COF-322, COF-330, COF-333, and COF-350 have a wider range of optimum pressure over bulk H_2 between 8 - 13 g/L from 100 - 700 bar. Only chelated COF-340 that have very large pore > 18 Å have uptake benefit less than 4 g/L over bulk H_2.

All COFs have maximum extra uptake relative to bulk H_2 at the optimum pressures (P_{opt}). This depends on the linker, chelated Tm, and pore size (Figure 8 and Table 4). COF-301 has the lowest P_{opt} because it has smallest pore size ~ 6 Å and the surface area get saturated at pressure 60 - 120 bar. Larger pores such as COF-322, COF-330, and COF-333 that have about twice the pore sizes of COF-301 can get P_{opt}= 240 bar. With medium pore size ~ 9 Å, COF-350 can reach P_{opt}=180 bar and COF-340 with pore size ~ 18 Å can get P_{opt}=240 bar. Thus there is a sweet spot of pore size that can have high extra uptake at high pressure. The surface area of the COF-301 is already saturated with the H_2 at 150 bar and the uptake of H_2 will be limited to the available volume of the system. Above this pressure, COF-301 alone and COF-301-MnCl2 have less total uptake than bulk H_2 (negative extra uptake). The smaller available volume with the addition of $MnCl_2$ cannot be compensated by the additional interaction between Mn(II) with H_2 at high enough pressure, this depends on the pore size of the COFs.

A way to explain this behavior besides the pore aperture and the density is to look at

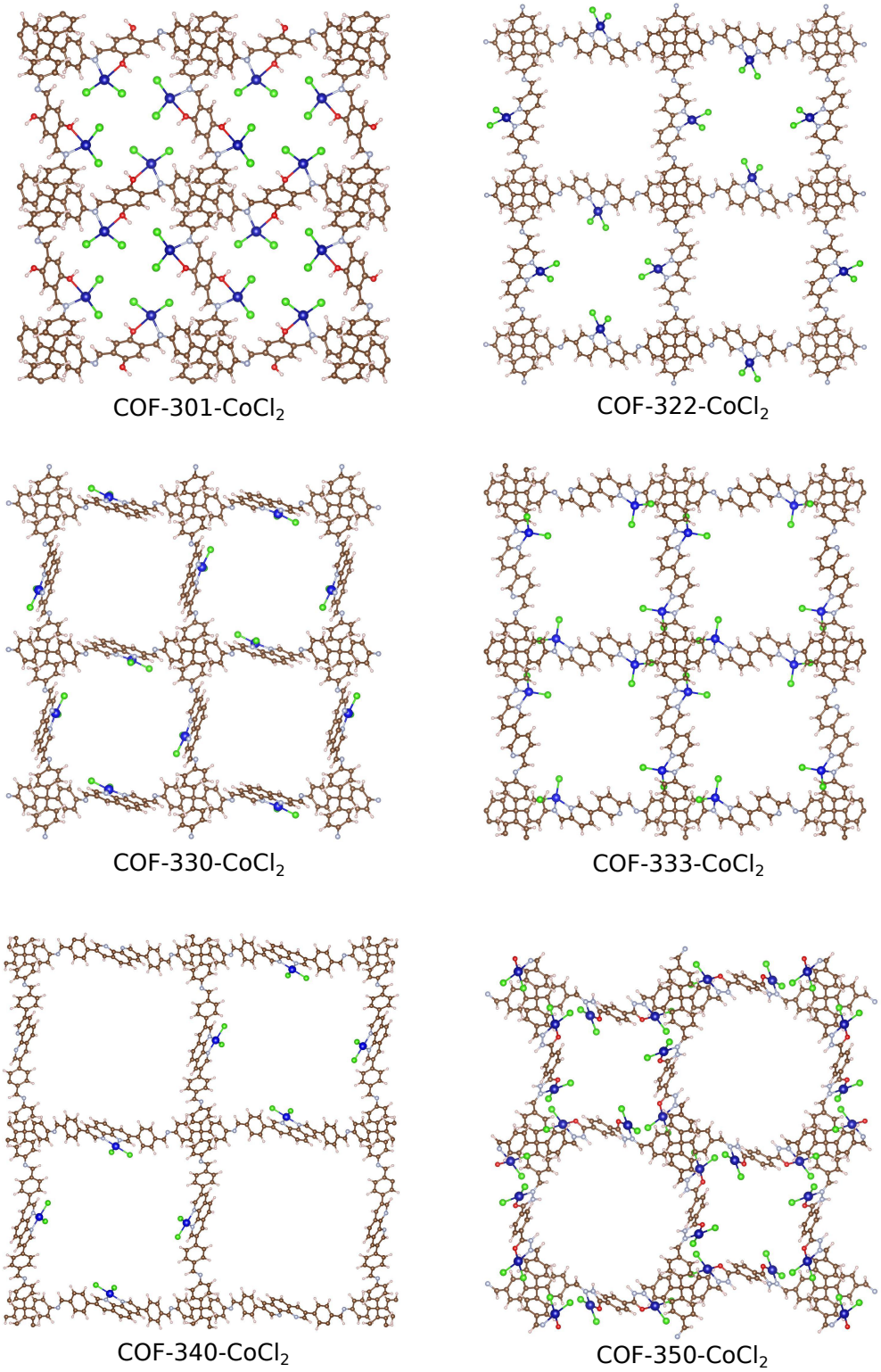

Figure 7: Chelated COF-301-$CoCl_2$, COF-322-$CoCl_2$, COF-330-$CoCl_2$, COF-333-$CoCl_2$, COF-340-$CoCl_2$, and COF-350-$CoCl_2$. The pore size and small distance between chelated sites can be tuned to allow H_2 to interact with all the $TmCl_2$ from neighboring layers, giving a 'cooperative effect'.

Table 4: Surface area ($S_A, \mathrm{m}^2/\mathrm{g}$), pore volume ($V_P\,, \mathrm{cm}^3/\mathrm{g}$), ($Q_{st}^{\mathrm{initial}}$, kJ/mol) from GCMC, binding enthalpy ($\Delta \mathrm{H}^{\circ}_{\mathrm{bind}}$, kJ/mol) from QM, pore size (P_{size}, Å), distance between neighboring framework layer (D_{layer}, Å) and saturation pressure (P_{opt}, bar) are presented.

							Extra H_2 at P_{opt}		
Structure	S_A	V_p	P_{size}	D_{layers}	$Q_{st}^{\mathrm{initial}}$	$\Delta \mathrm{H}^{\circ}_{\mathrm{bind}}$	P_{opt}	grav%	vol g/L
COF-300	3,700	1.30	10.3	8.89	5.83	5.90	100	1.38	0.795
COF-301	3,600	1.16	6.00	8.92	5.99	6.96	70.0	1.43	0.419
COF-320	6,700	2.52	13.5	12.2	4.41	5.83	160	1.05	1.06
COF-322	6,800	2.51	14.4	11.7	4.44	5.83	160	3.42	1.07
COF-330	3,600	2.50	15.6	12.7	4.79	5.62	180	3.31	1.40
COF-333	4,400	1.64	13.4	12.1	4.39	4.01	140	3.08	1.11
COF-340	9,200	4.55	21.9	16.4	3.64	5.62	220	6.81	0.668
COF-350	6,800	2.24	9.20	12.8	4.11	6.03	100	2.69	0.602
COF-301-$CoCl_2$	1,100	0.560	5.33	8.76	16.1	9.26	120	2.79	22.2
COF-301-$CuCl_2$	960	0.530	4.99	8.82	11.4	11.0	120	1.44	7.80
COF-301-$FeCl_2$	960	0.530	5.17	8.79	15.9	9.66	120	2.48	18.7
COF-301-$MnCl_2$	950	0.550	5.19	8.77	7.79	11.1	60.0	0.58	0.909
COF-301-$NiCl_2$	1,000	0.520	5.33	8.84	16.3	8.07	100	2.51	21.3
COF-322-$CoCl_2$	5,400	1.77	11.6	11.4	7.93	9.07	240	4.97	9.34
COF-322-$CuCl_2$	5,300	1.75	11.6	11.4	6.93	9.65	200	3.53	4.08
COF-322-$FeCl_2$	5,400	1.78	11.6	11.4	9.59	8.66	200	4.34	7.80
COF-322-$MnCl_2$	5,400	1.78	11.6	11.4	5.32	9.26	160	1.24	1.59
COF-322-$NiCl_2$	5,400	1.76	11.6	11.4	10.9	9.10	240	4.78	8.22
COF-330-$CoCl_2$	4,000	1.68	14.2	12.8	9.19	8.54	240	5.27	9.63
COF-330-$CuCl_2$	4,000	1.65	14.2	12.8	7.45	9.99	220	3.70	4.59
COF-330-$FeCl_2$	4,100	1.70	14.2	12.8	10.3	9.54	240	4.78	8.62
COF-330-$MnCl_2$	4,100	1.70	14.2	12.8	5.30	8.75	160	2.62	1.80
COF-330-$NiCl_2$	4,000	1.68	14.2	12.8	8.98	9.13	220	4.65	9.09
COF-333-$CoCl_2$	3,200	1.24	12.9	11.4	14.0	8.63	220	4.20	13.3
COF-333-$CuCl_2$	3,200	1.24	12.9	11.4	8.12	9.68	180	2.55	4.45
COF-333-$FeCl_2$	3,300	1.27	12.9	11.4	14.0	9.60	200	3.76	10.9
COF-333-$MnCl_2$	3,300	1.28	12.9	11.4	5.19	5.19	90.0	1.97	0.718
COF-333-$NiCl_2$	3,200	1.24	12.9	11.4	15.0	9.36	180	3.70	11.8
COF-340-$CoCl_2$	7,400	3.67	18.4	16.1	6.52	8.54	240	7.00	3.74
COF-340-$CuCl_2$	7,400	3.65	18.4	16.1	5.10	9.99	220	5.92	1.82
COF-340-$FeCl_2$	7,400	3.69	18.4	16.1	7.42	9.54	220	6.52	3.28
COF-340-$MnCl_2$	7,400	3.70	18.4	16.1	3.82	8.75	180	4.91	0.844
COF-340-$NiCl_2$	7,400	3.67	18.4	16.1	8.00	9.13	220	6.57	3.50
COF-350-$CoCl_2$	3,300	1.21	9.01	10.7	13.4	9.64	180	3.94	13.8
COF-350-$CuCl_2$	3,200	1.19	9.01	10.7	9.32	8.08	160	2.47	5.40
COF-350-$FeCl_2$	3,300	1.22	9.01	10.7	14.0	10.3	180	3.72	12.1
COF-350-$MnCl_2$	3,300	1.22	9.01	10.7	5.70	8.23	80.0	0.86	0.888
COF-350-$NiCl_2$	3,200	1.21	9.01	10.7	14.6	10.1	180	3.94	12.9

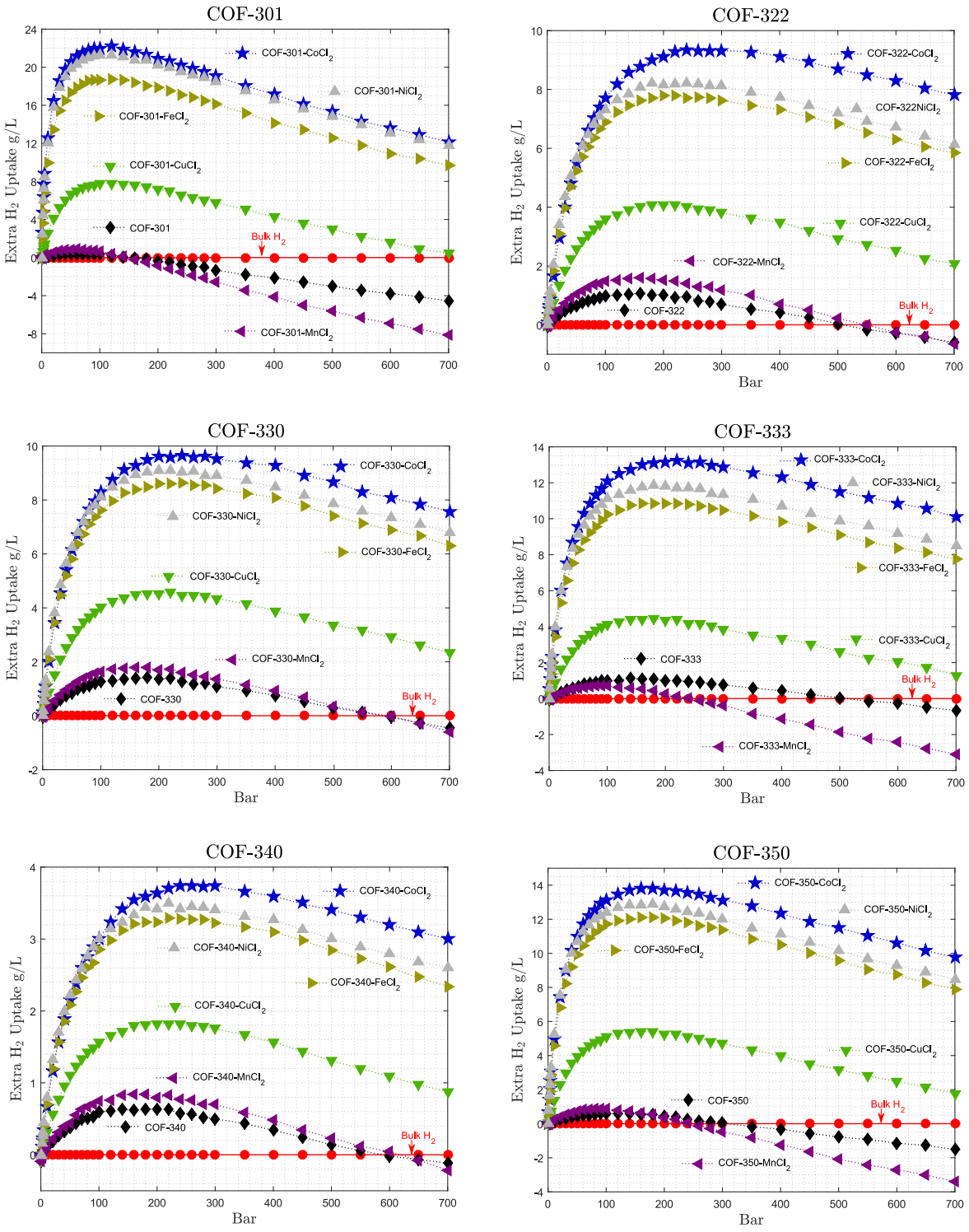

Figure 8: The relative uptake for COF-301, COF-322, COF-330, COF-333, COF-340, and COF-350 with different transition metals from bulk H_2.

the initial isosteric heat adsorption at 0-5 bar (Q_{st}^{initial}) values for each of the compounds. Because each COF is made basically of the same elements and type of connectivity, it would be expected to have the same kind of interaction with H_2. The Q_{st}^{initial} for all the pure COFs have a value between 4 and 6 kJ/mol (Table 4), which indicates that they have similar interaction with Tm. COF-301 has the lowest gravimetric uptake but the highest Q_{st}^{initial} because it has a small pore, therefore the potential energy surface for the pore overlaps and makes the H_2 interacts strongly with framework. However, the small pore limits the maximum amount of H_2 that can be adsorbed. Figure 8 shows the extra uptake of each structure to bulk H_2, smaller pores size has lower optimum pressure range relative to bulk H_2. It was postulated at the beginning that in general the Q_{st}^{initial} values are comparable to the binding enthalpy ($\Delta H^{\circ}_{\text{bind}}$) for the first 4 H_2 bounded to the linkers. This suggests that the estimation of the $\Delta H^{\circ}_{\text{bind}}$ of the linker can be used as a first approximation of the Q_{st}^{initial} for the periodic structure (Table 4). In Figure 4, a $\Delta H^{\circ}_{\text{bind}}$ of around 8 - 12 kJ/mol was described, however, this considers that the fraction of the organic part is smaller than in the framework, i.e. the concentration of Tm is smaller in the framework than in the ligand.

At 0-5 bar, COF-301-$TmCl_2$, COF-333-$TmCl_2$, COF-350-$TmCl_2$ have a higher value of Q_{st}^{initial} =13.4 kJ/mol - 16.3 kJ/mol while the $\Delta H^{\circ}_{\text{bind}}$ is 8.07 - 11.0 kJ/mol from QM on the isolated linker. It can be seen that the number of $TmCl_2$ is twice per linker in those COFs than in COF-322, COF-330, and COF-340 or isolated linker. However only COF-301-$TmCl_2$ such as Co(II) still has high Q_{st}=15.8 kJ/mol at 700 bar (shown in Supplementary Information SI). This high interaction energy is reflected in the general performance since COF-301-$CoCl_2$ reaches total extra uptake of 22 g/L at 120 bar above bulk H_2 (Figure 4 and Table 4). This is because the small distance between chelated sites in COF-301-$CoCl_2$ is ideal, allowing H_2 to interact with all the $CoCl_2$ from neighboring layers, giving a 'cooperative effect'. This cooperative effect is observed when the distance between chelated sites is less than 12 Å or close to the nanoporous regime. However if the pore is too small there will be no space to put Tm which makes the choice of linker critical to generate the ideal pore.

Thus, based on our results that short linkers, which generate COFs with small pores of around 6 Å to 12 Å, give rise to a 'cooperative effect' that is optimal for the use of space for Tm storage. The simplest chelation approach ($TmCl_2$) was used, and demonstrates that the same interaction enthalpy towards Tm can be obtained with other lighter and abundant Tm, thus reaching even higher gravimetric uptake is possible. Also, higher volumetric uptakes could be attained if the Tm is smaller with a square planar or tetrahedral geometry.

SUMMARY.

The first row Tm (Sc to Cu) can give similar and sometimes superior van der Waals interactions with H_2 than precious Tm (Pd and Pt). Based on these results, the long range non-bonding interactions depend poorly on the Tm oxidation state and even geometry of the coordination shell when there is no η^2-Tm formation. Most of these Tm fall in the ideal interaction range of 7-15 kJ/mol for maximum delivery and uptake. Thus, if the gravimetric uptake needs to be optimized, the lighter first row Tm can be used.

Previously the uptake of the precious Tm chelation had been predicted; such as $PdCl_2$, however it is demonstrated in this work that the same interaction enthalpy toward Tm can be obtained with any other lighter Tm, thus reaching even higher volumetric and gravimetric uptake is possible. These materials made of simple linkers overcome the 2020 DOE volumetric target of 40 g/L. The bulk H_2 alone can reach 40 g/L at 700 bar and 298K, but within this model, the total uptakes in chelated Co(II), Cu(II), Fe(II), and Ni(II) in COFs are consistently higher than bulk H_2 in wide pressure range (0-700 bar). In general, the Q_{st}^{initial} values for the framework are comparable to the binding enthalpy ($\Delta H^{\circ}_{\text{bind}}$) of the linkers. This correlates with the Tm uptake. Thus $\Delta H^{\circ}_{\text{bind}}$ can be used for the linker as a first approximation of the Q_{st}^{initial} of the periodic structure, assuming that the surface for interaction of the linkers is mostly exposed. However, the $\Delta H^{\circ}_{\text{bind}}$ does not consider the size of the pore and this gives rise to discrepancies when in the nanopore range.

Surface area and pore volume have been the main parameters to optimize for porous frameworks however it has been shown that they have a limit, especially for the excess gravimetric uptake and for the total volumetric uptake at room temperature.

ACKNOWLEDGMENTS

J.L.M.C. would like to acknowledge the start-up funds from Florida State University and the Energy and Material Initiative. J.L.M.C. and Y. P. acknowledge the High Performance Computer Center at Florida State University and facilities at the High Performance Material Institute. J.L.M.C. and Y. P. acknowledge Yubo Su for initial discussions.

ASSOCIATED CONTENT

Supporting Information Available

Optimized geometries at the Quantum Mechanical Level for the COFs as well as the gravimetric uptake of all the compounds are contained and available in the supplementary information.

AUTHOR INFORMATION

Corresponding Authors

J.L.M.C. E-mail: jmendozacortes@fsu.edu.

Notes

The authors declare no competing financial interests.

References

(1) USDOE Office of Energy Efficiency & Renewable Energy (EERE), l. *http://energy.gov/sites/prod/files/2015/05/f22/fcto_myrdd_storage.pdf* **2015**,

(2) Mendoza-Cortes, J. L.; Han, S. S.; Goddard, W. A. *J. Phys. Chem. A* **2012**, *116*, 1621–1631.

(3) Bhatia, S. K.; Myers, A. L. *Langmuir* **2006**, *22*, 1688–1700.

(4) Han, S. S.; Goddard, W. A. *J. Phys. Chem. C* **2008**, *112*, 13431–13436.

(5) Yoon, M.; Yang, S. Y.; Hicke, C.; Wang, E.; Geohegan, D.; Zhang, Z. Y. *Phys. Rev. Lett.* **2008**, *100*.

(6) Sun, Y. Y.; Lee, K.; Kim, Y. H.; Zhang, S. B. *Appl. Phys. Lett.* **2009**, *95*, 33109–4.

(7) Han, S. S.; Goddard, W. A. *J. Am. Chem. Soc.* **2007**, *129*, 8422–8423.

(8) Doonan, C. J.; Morris, W.; Furukawa, H.; Yaghi, O. M. *J. Am. Chem. Soc.* **2009**, *131*, 9492–9493.

(9) Bloch, E. D.; Britt, D.; Lee, C.; Doonan, C. J.; Uribe-Romo, F. J.; Furukawa, H.; Long, J. R.; Yaghi, O. M. *J. Am. Chem. Soc.* **2010**, *132*, 14382–14384.

(10) Mendoza-Cortes, J. L.; Goddard, W. A.; Furukawa, H.; Yaghi, O. M. *J. Phys. Chem. Lett.* **2012**, *3*, 2671–2675.

(11) Lochan, R. C.; Head-Gordon, M. *Phys. Chem. Chem. Phys.* **2006**, *8*, 1357–1370.

(12) Pascal, T. A.; Boxe, C.; Goddard, W. A. *J. Phys. Chem. Lett.* **2011**, *2*, 1417–1420.

(13) Kubas, G. J. *Chem. Rev.* **2007**, *107*, 4152–4205.

(14) Gonzalez, A. A.; Zhang, K.; Nolan, S. P.; Delavega, R. L.; Mukerjee, S. L.; Hoff, C. D.; Kubas, G. J. *Organometallics* **1988**, *7*, 2429–2435.

(15) Heinekey, D. M.; Voges, M. H.; Barnhart, D. M. *J. Am. Chem. Soc.* **1996**, *118*, 10792–10802.

(16) Shen, J. Y.; Haar, C. M.; Stevens, E. D.; Nolan, S. P. *J. Organomet. Chem.* **1998**, *571*, 205–213.

(17) Labet, V.; Hoffmann, R.; Ashcroft, N. W. *J. Chem. Phys.* **2012**, *136*, 074503–10.

(18) te Velde, G.; Bickelhaupt, F. M.; Baerends, E. J.; Fonseca Guerra, C.; van Gisbergen, S. J. A.; Snijders, J. G.; Ziegler, T. *J. Comput. Chem.* **2001**, *22*, 931–967.

(19) Gell, M.; Luis, J. M.; Sol, M.; Swart, M. *J. Phys. Chem. A* **2008**, *112*, 6384–6391.

(20) Uribe-Romo, F. J.; Doonan, C. J.; Furukawa, H.; Oisaki, K.; Yaghi, O. M. *J. Am. Chem. Soc.* **2011**, *133*, 11478–11481.

(21) Uribe-Romo, F. J.; Hunt, J. R.; Furukawa, H.; Klock, C.; O'Keeffe, M.; Yaghi, O. M. *J. Am. Chem. Soc.* **2009**, *131*, 4570–4571.

(22) Wu, H. P.; Janiak, C.; Rheinwald, G.; Land, H. *J. Chem. Soc. Dalton Trans.* **1999**, 183–190.

(23) Ghosh, M.; Biswas, P.; Florke, U.; Nag, K. *Inorg. Chem.* **2008**, *47*, 281–296.

(24) Osborn, R. S.; Rogers, D. *J. Chem. Soc. Dalton Trans.* **1974**, 1002–1004.

(25) Maekawa, M.; Munakata, M.; Kitagawa, S.; Nakamura, M. *Anal. Sci.* **1991**, *7*, 521–522.

TABLE OF CONTENTS GRAPHIC